Atmos. Chem. Phys., 18, 2481–2493, 2018
https://doi.org/10.5194/acp-18-2481-2018

Atmospheric Chemistry and Physics
Open Access

Multiphase oxidation of SO_2 by NO_2 on $CaCO_3$ particles

Defeng Zhao[1,*], Xiaojuan Song[1,*], Tong Zhu[1], Zefeng Zhang[1], Yingjun Liu[1], and Jing Shang[1]

[1] BIC-ESAT and SKL-ESPC, College of Environmental Sciences and Engineering, Peking University, Beijing, 100871, China
[*] These authors contributed equally to this work.

Correspondence: Tong Zhu (tzhu@pku.edu.cn)

Received: 29 June 2017 – Discussion started: 3 July 2017
Revised: 17 December 2017 – Accepted: 19 December 2017 – Published: 19 February 2018

Abstract. Heterogeneous/multiphase oxidation of SO_2 by NO_2 on solid or aqueous particles is thought to be a potentially important source of sulfate in the atmosphere, for example, during heavily polluted episodes (haze), but the reaction mechanism and rate are uncertain. In this study, in order to assess the importance of the direct oxidation of SO_2 by NO_2 we investigated the heterogeneous/multiphase reaction of SO_2 with NO_2 on individual $CaCO_3$ particles in N_2 using Micro-Raman spectroscopy. In the SO_2 / NO_2 / H_2O / N_2 gas mixture, the $CaCO_3$ solid particle was first converted to the $Ca(NO_3)_2$ droplet by the reaction with NO_2 and the deliquescence of $Ca(NO_3)_2$, and then NO_2 oxidized SO_2 in the $Ca(NO_3)_2$ droplet forming $CaSO_4$, which appeared as needle-shaped crystals. Sulfate was mainly formed after the complete conversion of $CaCO_3$ to $Ca(NO_3)_2$, that is, during the multiphase oxidation of SO_2 by NO_2. The precipitation of $CaSO_4$ from the droplet solution promoted sulfate formation. The reactive uptake coefficient of SO_2 for sulfate formation is on the order of 10^{-8}, and RH enhanced the uptake coefficient. We estimate that the direct multiphase oxidation of SO_2 by NO_2 is not an important source of sulfate in the ambient atmosphere compared with the SO_2 oxidation by OH in the gas phase and is not as important as other aqueous-phase pathways, such as the reactions of SO_2 with H_2O_2, O_3, and O_2, with or without transition metals.

1 Introduction

Sulfate is a major component of atmospheric particulate matter. It contributes to a large fraction of atmospheric aerosol particles in both urban and rural areas (Seinfeld and Pandis, 2006; Zhang et al., 2007). Sulfate either comes from primary sources, such as sea spray, or from secondary sources, i.e., from the oxidation of reduced sulfur compounds such as dimethyl sulfide (DMS), carbonyl sulfur (COS), and SO_2 (Seinfeld and Pandis, 2006). In the continental atmosphere, the main source of sulfate is the oxidation of SO_2, an important air pollutant from fossil fuel combustion. SO_2 can be oxidized in the gas phase, mainly by OH, or in the particle phase such as by H_2O_2, O_3, or O_2, catalyzed by transition metal ions in cloud or fog water (Seinfeld and Pandis, 2006; Finlayson-Pitts and Pitts Jr., 1999), or by O_3 or photochemical reactions on the particle surface (Zhu et al., 2011; Li et al., 2006, 2007, 2011; Shang et al., 2010).

Although various pathways of SO_2 oxidation are identified, the source of sulfate and relative importance of various pathways of SO_2 oxidation forming sulfate in the atmosphere still remain uncertain. For example, during heavily polluted episodes (haze) in China in recent years, high concentrations of sulfate were observed, but the source of sulfate is elusive (Wang et al., 2016; Y. S. Wang et al., 2014; G. J. Zheng et al., 2015; Guo et al., 2014). The relative contribution of regional transport versus local formation and the physical and chemical mechanisms responsible for sulfate formation are still not clear. Recent studies have highlighted heterogeneous reactions of SO_2 on solid or liquid particles as a possibly important source of sulfate based on model, field, and laboratory studies (Huang et al., 2014; Zhu et al., 2011; Gao et al., 2016; B. Zheng et al., 2015; Y. X. Wang et al., 2014, 2016; He et al., 2014; Fu et al., 2016; Xue et al., 2016; Xie et al., 2015; Cheng et al., 2016). During haze episodes, relative humidity (RH) is often high (Zhang et al., 2014; Wang et al., 2016; G. J. Zheng et al., 2015), and particles or some components of particles can deliquesce, forming aqueous solutions. In particular, several recent studies propose that the multiphase oxidation of SO_2 by NO_2, another important air pollutant, on liquid particles may be a major pathway of sulfate formation (Wang et al., 2016; Xue et al., 2016; Xie et al., 2015; Cheng et al., 2016). Both SO_2 and NO_2 are from fossil fuel combustion and both concentrations are often high during haze episodes, and their reaction may significantly contribute to sulfate formation.

In order to assess and quantify the role of the heterogeneous reactions of SO_2 in sulfate formation, laboratory studies are needed to understand the reaction process and obtain kinetic parameters for modeling, such as uptake coefficients of SO_2. Among many studies investigating the heterogeneous reactions of SO_2 on various particles (Goodman et al., 2001; Li et al., 2011, 2004, 2006; Shang et al., 2010; Huang et al., 2015, 2016; Zhou et al., 2014; Kong et al., 2014; Passananti et al., 2016; Cui et al., 2008; Chu et al., 2016; Zhao et al., 2015; Wu et al., 2011, 2013, 2015 He et al., 2014; Liu et al., 2012; Ma et al., 2008; Park and Jang, 2016; Ullerstam et al., 2002, 2003; Sorimachi et al., 2001), only a few have investigated the heterogeneous reaction of SO_2 in the presence of NO_2 (He et al., 2014; Liu et al., 2012; Ma et al., 2008, 2017; Park and Jang, 2016; Ullerstam et al., 2003). These studies found that NO_2 can promote sulfate formation from SO_2 oxidation (He et al., 2014; Liu et al., 2012; Ma et al., 2008; Park and Jang, 2016; Ullerstam et al., 2003). However, the mechanism of this effect is still not clear and only few studies reported kinetic parameters such as uptake coefficients of SO_2 due to the reaction with NO_2. Importantly, most of these studies focused on the gas–solid reactions on particles. Very few laboratory studies have investigated the multiphase reaction of SO_2 with NO_2 on atmospheric aqueous particles or solid–aqueous mixed-phase aerosol particles, and the uptake coefficient of SO_2 on atmospheric aqueous particles due to the reaction with NO_2 is largely unknown. From several decades ago until now, a number of studies have investigated the aqueous reaction of soluble S(IV) species (H_2SO_3, HSO_3^-, SO_3^{2-}) with NO_2 in dilute bulk solution (Lee and Schwartz, 1983; Clifton et al., 1988; Littlejohn et al., 1993; Takeuchi et al., 1977; Nash, 1979; Ellison and Eckert, 1984; Shen and Rochelle, 1998; Tursic and Grgic, 2001) relevant to the conditions in cloud water. However, in aqueous aerosol particles, the reaction rate and process may be substantially different from those in bulk solution due to high ionic strength resulted from high concentrations of solutes, potential interactions of sulfate with other ions, and low water activity in aerosol particles.

In this study, we present the finding that the multiphase reaction of SO_2 directly with NO_2 is not an important source of sulfate in the atmosphere, in the absence of other oxidants such as O_2. The direct oxidation of SO_2 by NO_2 pathway was proposed in a number of recent studies to be potentially important for sulfate formation (Cheng et al., 2016; Wang et al., 2016; Xue et al., 2016). For example, Cheng et al. (2016) considered the direct oxidation of SO_2 by NO_2 to be the most important pathway to explain the missing sulfate source during haze events in Beijing. Wang et al. (2016) also proposed that the direct oxidation of SO_2 by NO_2 is key to efficient sulfate formation in the presence of high relative humidity and NH_3 and showed that in their laboratory study sulfate formation is mainly contributed by the direct oxidation by NO_2 and that the role of O_2 is negligible.

We investigated the heterogeneous reaction of SO_2 with NO_2 on $CaCO_3$ particles at ambient RH. $CaCO_3$ is an important component of mineral aerosols, especially in East Asia (Cao et al., 2005; Song et al., 2005; Okada et al., 2005), and it is a very reactive component (Krueger et al., 2004; Li et al., 2010, 2006; Prince et al., 2007a). It is also one of the few alkaline particles in the atmosphere, especially in northern China, which can neutralize acids on particles and increase the pH of aerosol water, thus promoting the apparent solubility and uptake of SO_2. The reaction of SO_2 with NO_2 on $CaCO_3$ has been suggested by field observations, which showed internal mixing of $CaCO_3$, $CaSO_4$, and $Ca(NO_3)_2$ in particles (Hwang and Ro, 2006; Li and Shao, 2009; Zhang et al., 2000). More importantly, as shown below, during the reaction on $CaCO_3$, the aqueous phase can be formed, which allows us to investigate the multiphase reaction of SO_2 with NO_2. We studied the reaction of SO_2 and NO_2 on individual $CaCO_3$ particles in N_2 using a Micro-Raman spectrometer with a flow reaction system. N_2 was used as a carrier gas in order to avoid confounding effects of other oxidants including O_2 in SO_2 oxidation. Combining the chemical and optical information from the Micro-Raman spectrometer, we systematically investigated the reaction process and quantified the reactive uptake coefficient of SO_2 due to the oxidation by NO_2 based on the sulfate production rate. We further assessed the importance of the multiphase oxidation of SO_2 by NO_2 in the atmosphere.

2 Experimental

2.1 Apparatus and procedures

The experimental setup used in this study is illustrated in Fig. 1. The details of the setup have been described previously (Liu et al., 2008; Zhao et al., 2011). NO_2 and SO_2 of certain concentrations were prepared by adjusting the flow rates of standard gases of specified concentrations (NO_2: 1000 ppm in N_2, Messer, Germany; SO_2: 2000 ppm in N_2, National Institute of Metrology P.R. China) and high-purity nitrogen (99.999 %, Beijing Haikeyuanchang Corp.). We used N_2 as a carrier gas to exclude the potential inference from other compounds in SO_2 oxidation such as O_2, which is key to investigate the direct oxidation of SO_2 by NO_2. RH was regulated by adjusting the flow rates of humidified N_2 and of dry N_2 and other dry gases. Humidified N_2 was prepared by bubbling N_2 through fritted glass in water. Flow rates of the gases were controlled by mass flow controllers (FC-260, Tylan, Germany). Mixed gases reacted with $CaCO_3$ particles in a stainless steel reaction cell. Individual $CaCO_3$ particles were deposited on a Teflon™ FEP film substrate an-

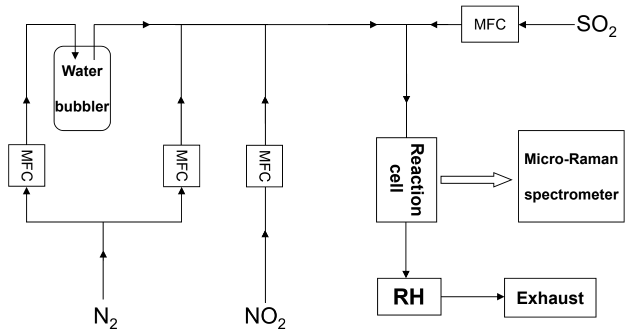

Figure 1. Schematic diagram of the experimental setup. MFC: mass flow controller.

nealed to a silicon wafer. The substrate was then placed in the reaction cell, which has a glass cover on top of the center. Through this top window, a Micro-Raman spectrometer (LabRam HR800, HORIBA Jobin Yvon) was used to acquire the Raman spectra of particles. A 514 nm excitation laser was focused onto selected particles, and back scattering Raman signals were detected. The details of the instrument have been described in previous studies (Liu et al., 2008; Zhao et al., 2011).

The RH and temperature of the outflow gas from the reaction cell were measured by a hygrometer (HMT100, Vaisala). Experiments of individual $CaCO_3$ particles reacting with NO_2 (75–200 ppm) and SO_2 (75–200 ppm) mixing gas diluted with N_2 were conducted under certain RH (17–72 %). All the measurements were carried out at 25 ± 0.5 °C. Each reaction was repeated three times.

In this study, the size of $CaCO_3$ particles was around 7–10 µm. During a reaction, components of an individual particle may distribute unevenly within the particle due to the formation of a new aqueous phase or solid phase, and particles may grow. Because particles are larger than the laser spot (~ 1.5 µm), the Raman spectrum from one point does not represent the chemical composition of the whole particle. Therefore Raman mapping was used to obtain the spectra on different points of a particle in order to obtain the chemical information of the whole particle. The mapping area is a rectangle slightly larger than the particle, and mapping steps are 1×1 µm. Raman spectra in the range 800–3900 cm^{-1} were acquired with an exposure time of 1 s for each mapping point. During each mapping period (7–10 min, depending on the mapping area), no noticeable change in composition was detected. The mean time of a mapping period was used as the reaction time. During the reaction, microscopic images of particles were also recorded. Raman spectra were analyzed using Labspec 5 software (HORIBA Jobin Yvon). Raman peaks were fit to Gaussian–Lorentzian functions to obtain peak positions and peak areas on different points of the particle. The peak areas were then added up to calculate the peak area for the whole particle.

Besides the reaction of $CaCO_3$ with SO_2 and NO_2, other reaction systems including the reaction on $Ca(NO_3)_2$, $NaNO_3$, and NH_4NO_3 particles with SO_2 or SO_2 and NO_2 mixing gas (summarized in Table 1) were also studied in order to elucidate the reaction mechanism. Most experiments were conducted using $CaCO_3$ particles rather than directly using $Ca(NO_3)_2$ particles. $CaCO_3$ was selected because it is an important component of mineral aerosols, especially in China as mentioned in the Introduction, and it is often used as a surrogate of mineral aerosols. Moreover, using $CaCO_3$ particles can better simulate the reaction on internally mixed $CaCO_3$(solid)–$Ca(NO_3)_2$(aqueous) particles, which is widely observed in the ambient atmosphere and laboratory (Laskin et al., 2005; Zhang et al., 2003; Li and Shao, 2009; Sullivan et al., 2007; Li et al., 2010; Liu et al., 2008), and it is formed via the reaction of $CaCO_3$ with acidic gases such as HNO_3 and NO_2 due to its alkalinity.

$CaCO_3$ (98 %, Sigma) with diameters about 7–10 µm on average, $Ca(NO_3)_2 \cdot 4H_2O$ (ACS, 99–103 %; Riedel-de Haën), NH_4NO_3 (AR, Beijing Chemical Works), and $NaNO_3$ (AR, Beijing Chemical Works) were used without further purification.

2.2 Quantification of reaction products on the particle phase

The Raman intensity of a sample is described in Eq. (1):

$$I(\nu) = I_0 \cdot A(\nu) \cdot J(\nu) \cdot \nu^4 \cdot D \cdot K, \qquad (1)$$

where I_0 is the intensity of incident laser, $A(\upsilon)$ is the collection efficiency function of a Raman spectrometer, $J(\upsilon) \cdot \upsilon^4$ is the Raman scattering section of the sample, D is the number density of the sample, and K is the effective depth of the sample. Raman intensity is not only determined by the amount of the sample molecules, but also by the configuration of the instrument, whose influence cannot be eliminated unless internal standards are used. For soluble compounds, water can be used an internal standard (Zhao et al., 2011; Liu et al., 2008). However, in this study, one product ($CaSO_4$; see below) appeared in a solid state. For solid particles of micro-scale, it is hard to add internal standards into the system. Therefore it is difficult to establish the relationship between Raman intensity and the number of sample molecules, which makes the quantification very challenging.

In this study, we chose seven individual $CaSO_4$ particles varying in size as the standard for solid products. The profile of each particle can be obtained by scanning the particle using Raman mapping with steps of 1, 1, and 2 µm for x, y, and z dimensions, respectively. The volume of each particle was calculated based on 3-D profiles of the particles using CAD software (AutoDesk). In order to minimize the influence of variations of incident laser on Raman intensity, these seven particles were measured before each experiment, which produced a calibration curve for each experiment (Fig. S1 in the Supplement).

Table 1. Summary of the results obtained in different reaction systems.

Particle	Gases	RH (%)	Whether sulfate was detected
$CaCO_3$	SO_2(75 ppm) + NO_2(75 ppm)	72	Yes
$Ca(NO_3)_2$ droplet	SO_2(75 ppm) + NO_2(75 ppm)	72	Yes
$CaCO_3$	SO_2(150 ppm)	72	No
$Ca(NO_3)_2$ droplet	SO_2(150 ppm)	72	No
$NaNO_3$ droplet	SO_2(75 ppm) + NO_2(75 ppm)	72	No
NH_4NO_3 droplet	SO_2(75 ppm) + NO_2(75 ppm)	72	No

2.3 Determination of reactive uptake coefficient

In this study, sulfate was produced from the oxidation of SO_2. The reactive uptake coefficient γ of SO_2 on individual particles was estimated from sulfate formation. γ is derived as the rate of sulfate formation $\left(\mathrm{d}\left\{SO_4^{2-}\right\}/\mathrm{d}t\right)$ divided by the rate of surface collisions with an individual particle (Z):

$$\gamma = \frac{\frac{\mathrm{d}\left\{SO_4^{2-}\right\}}{\mathrm{d}t}}{Z}, \tag{2}$$

$$Z = \frac{1}{4} c A_\mathrm{s}[SO_2], \tag{3}$$

$$c = \sqrt{\frac{8RT}{\pi M_{SO_2}}}, \tag{4}$$

where R is the gas constant, T is temperature, M_{SO_2} is the molecular weight of SO_2, and c is the mean molecular velocity of SO_2, A_s is the surface area of an individual particle. Z is the collision rate between SO_2 and a particle. $\left\{SO_4^{2-}\right\}$ indicates the amount of sulfate in the particle phase in moles, and $[SO_2]$ indicates the concentration of SO_2 in the gas phase.

$\left\{SO_4^{2-}\right\}$ was determined by a calibration curve as stated above. In this study, since sulfate was mainly formed after the formation of a $Ca(NO_3)_2$ droplet as shown below, A_s was calculated by estimating the diameter of the droplet according to its microscopic image and using a shape of spherical segment defined by the contact angle of a water droplet on Teflon™ (Good and Koo, 1979). For each experiment, at least three particles with different diameters were measured to obtain an average reactive uptake coefficient.

3 Results and discussion

3.1 Reaction products and particle morphology changes

Figure 2 shows typical Raman spectra of a $CaCO_3$ particle during the reaction with SO_2 and NO_2. The peak at 1087 cm^{-1} is assigned to the symmetric stretching mode of carbonate (ν_1) (Nakamoto, 1997), which could be detected during the initial stage of the reaction. Shortly after the reaction started, a peak at 1050 cm^{-1} was observed, which is attributed to the symmetric stretching mode of nitrate (ν_1). This demonstrates that calcium nitrate ($Ca(NO_3)_2$) was produced during the reaction. A broad band at 2800–3800 cm^{-1} was also observed together with the formation of $Ca(NO_3)_2$. It is assigned to −OH stretching of water in aqueous solution. The formation of aqueous solution is attributed to the deliquescence of $Ca(NO_3)_2$, which is very hygroscopic and can deliquesce at ~ 10 % RH (Liu et al., 2008; Al-Abadleh et al., 2003; Tang and Fung, 1997). After about 82 min, a new peak at 1013 cm^{-1} was observed, which is attributed to the symmetric stretching mode of sulfate (ν_1) in anhydrite ($CaSO_4$) (Sarma et al., 1998). This peak clearly demonstrates that sulfate was formed. $CaSO_4$ as a reaction product has also been found in the reaction of $CaCO_3$ with SO_2 and NO_2 in a previous study (Q. X. Ma et al., 2013). Afterwards, no other Raman peaks than those of $CaCO_3$, $Ca(NO_3)_2$, and $CaSO_4$ were detected until 1050 min after the reaction.

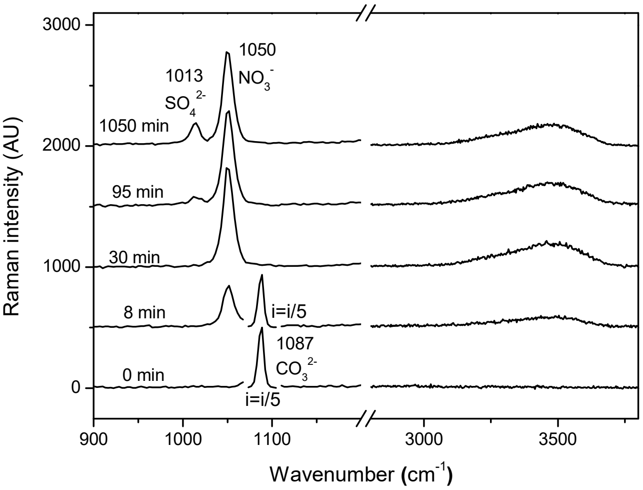

Figure 2. Raman spectra of an individual $CaCO_3$ particle during the reaction with NO_2 (75 ppm) and SO_2 (75 ppm) at 72 % RH at the reaction time of 0, 8, 30, 95, and 1050 min.

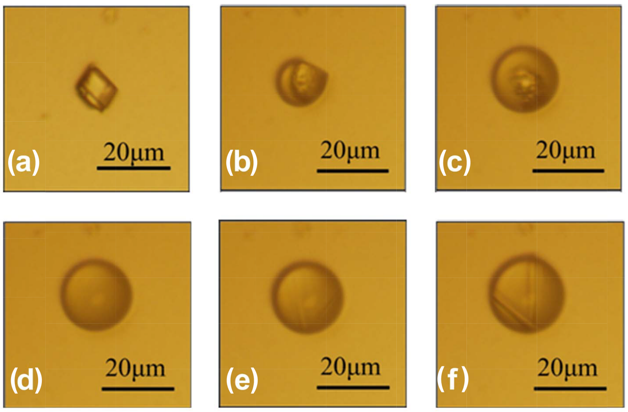

Figure 3. Microscopic images of an individual $CaCO_3$ particle (same as in Fig. 2) reacting with NO_2 (75 ppm) and SO_2 (75 ppm) at 72 % RH. Panels **(a–f)** correspond to the reaction time of 0, 6, 29, 37, 94, and 1050 min, respectively.

Concomitant with the formation of $Ca(NO_3)_2$ and $CaSO_4$, the microscopic morphology of the particle changed significantly. The initial $CaCO_3$ particle was a crystal close to a rhombohedron of about 9–10 μm (Fig. 3a). After reacting with NO_2 / SO_2, the surface of the particle became smoother, and then a liquid layer formed, surrounding the solid particle core (Fig. 3c). Raman spectra of the particle reveal that the outer liquid layer consisted of $Ca(NO_3)_2$ and water. As the reaction proceeded, the solid $CaCO_3$ core diminished gradually, and finally $CaCO_3$ completely disappeared and a $Ca(NO_3)_2$ spherical droplet was formed (Fig. 3d). The whole particle became larger due to the growth of the outer liquid layer. The diameter of the $Ca(NO_3)_2$ droplet reached ~ 16 μm, and the droplet did not change much in the subsequent period of the reaction. Despite the invariant droplet diameter, a new solid phase of needle-shaped crystals was formed as the reaction proceeded, which distributed unevenly in the droplet. The Raman spectra of the new solid phase and Raman mapping (Fig. S2) reveal that this solid matter was $CaSO_4$. The amount of $CaSO_4$ increased gradually during the reaction, and its Raman peak could be observed more clearly at 1050 min.

3.2 Reaction process

In order to learn about the reaction process and mechanism, the amounts of $Ca(NO_3)_2$, $CaSO_4$, and $CaCO_3$, represented by the peak area at 1050, 1013, and 1087 cm^{-1} in Raman spectra, respectively, were investigated as a function of reaction time. As shown in Fig. 4, $Ca(NO_3)_2$ was produced before $CaSO_4$. Nitrate was detected immediately after the reaction started, and it reached a maximum at ~ 50 min, whereas sulfate did not reach the detection limit until 82 min of the reaction. Sulfate increased slowly in the reaction and we did not observe it leveling off, even after 1050 min.

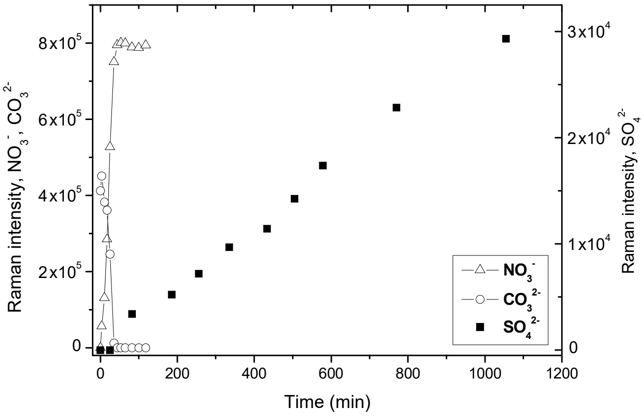

Figure 4. Raman peak intensity of carbonate, nitrate (left axis), and sulfate (right axis) as a function of time during the reaction of an individual $CaCO_3$ particle with NO_2 (75 ppm) and SO_2 (75 ppm) at 72 % RH (same as in Figs. 2 and 3). Note that the scales of the left axis and right axis are different. The intensity of NO_3^-, SO_4^{2-}, and CO_3^{2-} show the peak area at 1050, 1013, and 1087 cm^{-1}, respectively, in Raman spectra obtained by Raman mapping. By 118 min, $CaCO_3$ was completely converted to $Ca(NO_3)_2$. Carbonate had decreased to zero and nitrate had reached a plateau. Therefore no further data of carbonate and nitrate were shown.

According to the time series of carbonate, nitrate, and sulfate, this reaction consisted of two successive processes. The first process was the formation of $Ca(NO_3)_2$, which was accompanied by the decline of $CaCO_3$ (Fig. 4), indicating that $Ca(NO_3)_2$ was produced due to the reaction of $CaCO_3$ with NO_2. $Ca(NO_3)_2$ has been observed in the reaction of $CaCO_3$ with NO_2 in previous studies (Li et al., 2010; Tan et al., 2017). The formation of $Ca(NO_3)_2$ started with the reaction of NO_2 with adsorbed water or water in aqueous solution, forming HNO_3 and HNO_2. Then HNO_3 reacted with $CaCO_3$, forming $Ca(NO_3)_2$ as well as CO_2, which was released to the gas phase. HNO_2 could evaporate into the gas phase due to the continuous flushing of reactant gases during the experiments and acidity of the droplet (see below). The reaction equations are as follows.

$$NO_2\,(g) \leftrightarrow NO_2\,(aq) \tag{R1}$$

$$2NO_2\,(aq) + H_2O\,(aq) \rightarrow HNO_3\,(aq) + HNO_2\,(aq) \tag{R2}$$

$$HNO_3\,(aq) \rightarrow H^+\,(aq) + NO_3^-\,(aq) \tag{R3}$$

$$CaCO_3\,(s) + H^+\,(aq) \rightarrow Ca^+\,(aq) + HCO_3^-\,(aq) \tag{R4}$$

$$HCO_3^-\,(aq) + H^+\,(aq) \rightarrow H_2O\,(aq) + CO_2\,(g) \tag{R5}$$

$$HNO_2\,(aq) \leftrightarrow HNO_2\,(g) \tag{R6}$$

The detailed mechanisms of the formation of $Ca(NO_3)_2$ in the reaction $CaCO_3$ with NO_2 have been studied by Li et al. (2010).

The second process was the formation of $CaSO_4$ through the oxidation of SO_2 by NO_2. $CaSO_4$ was mainly produced after $CaCO_3$ was completely reacted and increased steadily as the reaction proceeded. The amount of $Ca(NO_3)_2$ as the product of NO_2 uptake was overwhelmingly higher than that of $CaSO_4$ as the product of the reaction of SO_2 with NO_2, which only reached detection limit after the complete conversion of $CaCO_3$. This indicates that the reaction of SO_2 with NO_2 did not contribute significantly to NO_2 uptake before $CaCO_3$ completely converted to $Ca(NO_3)_2$. Afterwards, the reaction of SO_2 with NO_2 promoted the reactive uptake of NO_2 by the $Ca(NO_3)_2$ droplet.

3.3 Reaction mechanism

3.3.1 Mechanism of sulfate formation

Based on the results above, we found that a series of reactions of SO_2 and NO_2 on a $CaCO_3$ particle led to sulfate formation. Almost the entire sulfate was produced after a $CaCO_3$ particle was converted to a $Ca(NO_3)_2$ droplet (Fig. 4); although in some experiments, a trace amount of sulfate could be observed when a small amount of $CaCO_3$ was still left in the $Ca(NO_3)_2$ droplet. The absence or low amount of sulfate before $CaCO_3$ was completely reacted might be due to the competition between the reaction of aqueous NO_2 with $CaCO_3$ and the reaction with SO_2. This result suggests that forming a $Ca(NO_3)_2$ droplet was key to the formation of sulfate.

This finding is further supported by the results of the reaction of SO_2 with NO_2 on a $Ca(NO_3)_2$ droplet (Fig. 5 and Table 1). Using a $Ca(NO_3)_2$ droplet as the reactant, the reaction with SO_2 / NO_2 in the same conditions still produced $CaSO_4$, confirming $CaCO_3$ was not necessary for sulfate formation. The reaction with $Ca(NO_3)_2$ produced a similar amount of sulfate to the reaction with $CaCO_3$ based on Raman spectra and microscopic images (Fig. 5), which indicates that the $Ca(NO_3)_2$ droplet was important for sulfate formation. Therefore, we conclude that SO_2 was mainly oxidized via the multiphase reaction on the $Ca(NO_3)_2$ droplet, while $CaCO_3$ mainly worked as a precursor of the $Ca(NO_3)_2$ droplet.

The oxidant of SO_2 can be NO_3^- or NO_2 in the $Ca(NO_3)_2$ droplet here. In a reaction between $Ca(NO_3)_2$ droplets and SO_2 (150 ppm) under 72 % RH, we did not observe any sulfate formation on the basis of the Raman spectra and microscopic image after 5 h of reaction. This indicates that NO_3^- was not the oxidant for SO_2 in our study, which was also consistent with a previous study (Martin et al., 1981). Therefore, we conclude that SO_2 was oxidized by NO_2 in the $Ca(NO_3)_2$ droplet.

According to previous studies, NO_2 can oxidize sulfite and bisulfite ions into sulfate ions in the aqueous phase (Ellison and Eckert, 1984; Shen and Rochelle, 1998; Littlejohn et al., 1993). The overall reaction equation was described to be as follows (Clifton et al., 1988):

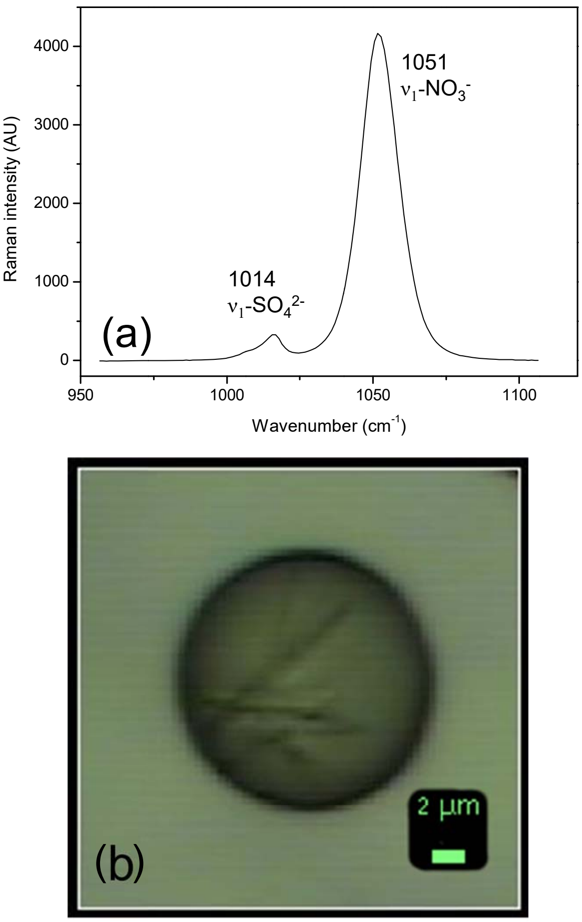

Figure 5. Raman spectra **(a)** and microscopic image **(b)** of a $Ca(NO_3)_2$ droplet reacting with NO_2 (75 ppm) and SO_2 (75 ppm) at 72 % RH at a reaction time of 300 min. The peak at 1014 cm^{-1} in Raman spectra and crystals from the microscopic image indicate $CaSO_4$ was formed in this reaction.

$$2NO_2\,(aq) + SO_3^{2-}\,(aq) + H_2O \longrightarrow 2H^+ + 2NO_2^-\,(aq) + SO_4^{2-}\,(aq) \tag{R7}$$

$$2NO_2\,(aq) + HSO_3^-\,(aq) + H_2O \longrightarrow 3H^+ + 2NO_2^-\,(aq) + SO_4^{2-}\,(aq)\,. \tag{R8}$$

Under the experimental conditions of our study, water uptake of $Ca(NO_3)_2$ led to condensation of water, which provided a site for aqueous oxidation of S(IV) by NO_2. The relative fractions of the three S(IV) species depend on pH, and the equilibrium between them is fast (Seinfeld and Pandis, 2006). The pH of the droplet was mainly determined by the gas–aqueous equilibrium of SO_2 in this study and was estimated to be ~ 3. The characteristic time to reach the equilibrium in the gas–particle interface ($\sim 10^{-5}$ s) was estimated to be much less than the characteristic time for the aqueous-phase reaction of SO_2 with NO_2 (10^{-2}–10^{-1} s) (Sect. S2 in the

Supplement). Therefore, aqueous S(IV) species can be considered to be in equilibrium with SO_2 in the gas phase. The concentrations of HSO_3^-, H_2SO_3, and SO_3^{2-} were estimated to be $\sim 1.1 \times 10^{-3}$, 9.2×10^{-5}, and $6.6 \times 10^{-8}\,\mathrm{mol\,L^{-1}}$, respectively, using the equilibrium constants in Seinfeld and Pandis (2006) ($H_{SO_2} = 1.23\,\mathrm{mol\,L^{-1}\,atm^{-1}}$, $K_1 = 1.3 \times 10^{-2}\,\mathrm{mol\,L^{-1}}$, $K_2 = 6.6 \times 10^{-8}\,\mathrm{mol\,L^{-1}}$), and thus the main S(IV) species was HSO_3^-. Then SO_4^{2-} from S(IV) oxidation can react with Ca^{2+}, forming $CaSO_4$ precipitation, as observed in Raman spectra due to the low value of K_{sp} for $CaSO_4$ (Lide, 2009):

$$Ca^{2+}\,(aq) + SO_4^{2-}\,(aq)\,CaSO_4\,(s)\,. \tag{R9}$$

Some previous studies have shown that SO_2 can react with $CaCO_3$ to produce calcium sulfite ($CaSO_3$) (Li et al., 2006; Prince et al., 2007b; Q. Ma et al., 2013), and $CaSO_3$ can be oxidized to $CaSO_4$ by NO_2 (Rosenberg and Grotta, 1980; Q. Ma et al., 2013). In our study, we investigated the reaction between $CaCO_3$ and SO_2 (150 ppm) at 72 % RH. We found that both sulfate and sulfite were lower than the detection limit of our Raman spectrometer ($\sim 5 \times 10^{-14}$ mol for sulfate at a signal-to-noise ratio of 2 and $\sim 3 \times 10^{-14}$ mol for sulfite according to the relative Raman scattering cross-section of sulfate and sulfite; Meyer et al., 1980), even after 300 min of the reaction. This indicates that forming $CaSO_3$ was not the main pathway in $CaSO_4$ formation in our study and that $CaCO_3$ did not directly contribute to the formation of $CaSO_4$.

3.3.2 Effects of cations in sulfate formation

Since sulfate was observed to precipitate as $CaSO_4$, we further analyzed the effect of precipitation reaction and cations on the aqueous oxidation of SO_2 by NO_2. In order to test effects of cations, we replaced Ca^{2+} with Na^+ or NH_4^+. Based on Raman spectra, we found that in the reaction of an $NaNO_3$ or an NH_4NO_3 droplet with NO_2 / SO_2, sulfate, either as aqueous ions (at 984 and 979 $\mathrm{cm^{-1}}$ for $(NH_4)_2SO_4$ and Na_2SO_4, respectively) or as $CaSO_4$ crystals, was below the detection limit after 300 min in the same reaction conditions as $Ca(NO_3)_2$ and $CaCO_3$ (Fig. 6 and Table 1). Considering that the Raman scattering cross-section of sulfate in $(NH_4)_2SO_4$ aqueous aerosol particles is even higher than sulfate in $CaSO_4$ (Wright, 1973; Stafford et al., 1976), it can be concluded that the sulfate production rate was larger in the presence of Ca^{2+} compared to that in the presence of Na^+ or NH_4^+. The difference can be explained by two possible reasons. The first possible reason may be due to the change of Gibbs energy. The spontaneity of the SO_2 oxidation by NO_2 for Reaction (R8) can be analyzed using the reaction Gibbs energy as follows:

$$\Delta_r G = \Delta_r G^\theta + RT \ln \frac{a_{H^+} \cdot a_{SO_4^{2-}} \cdot a_{NO_2^-}^2}{a_{NO_2(aq)}^2 \cdot a_{HSO_3^-}}, \tag{5}$$

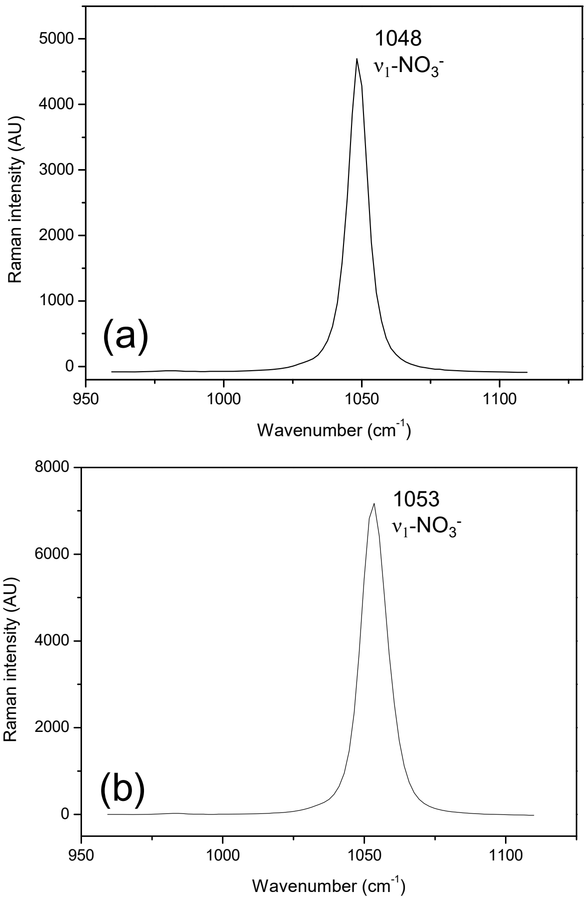

Figure 6. Raman spectra of a NH_4NO_3 **(a)** and $NaNO_3$ **(b)** droplet reacting with NO_2 (75 ppm) and SO_2 (75 ppm) at 72 % RH at the reaction time of 300 min.

where $\Delta_r G$ is the reaction Gibbs energy, $\Delta_r G^\theta$ is the standard reaction Gibbs energy, R is the gas constant, T is temperature, and a is the activity of various species.

$\Delta_r G$ increases with increasing sulfate concentration. According to the different results between the reaction on the $Ca(NO_3)_2$ droplet and the reaction on $NaNO_3$ and NH_4NO_3 droplets, there might be a backward reaction of SO_2 oxidation which consumed sulfate; although the detailed mechanism of the backward reaction is unknown at the moment. For $NaNO_3$ and NH_4NO_3 droplets, once sulfate concentration reached a certain level, the reaction may stop due to the increase of $\Delta_r G$. For $Ca(NO_3)_2$ droplets, the precipitation of $CaSO_4$ can substantially decrease the activity of SO_4^{2-} and thus decrease $\Delta_r G$ and promote the oxidation of SO_2 and sulfate formation. The second possible reason is that sulfate may crowd the reaction environment and suppress the colliding probability of S(IV) species with NO_2 in the aqueous phase and the uptake coefficient of SO_2 or NO_2 on the droplets. The precipitation of sulfate as $CaSO_4$ can cancel such suppression and thus promote the reaction. Regardless

Table 2. Reactive uptake coefficient of SO_2 for sulfate formation (γ) during the reaction of SO_2 with NO_2 on individual $CaCO_3$ particles under different conditions at 298 K.

$[SO_2]$ (ppm)	$[NO_2]$ (ppm)	RH (%)	γ ($\times 10^{-8}$)
75	75	72	3.22 ± 1.08^b
75	200	72	16.0 ± 3.12
75	75	46	3.22 ± 0.90
75	75	17	0^a
200	200	17	0^a

[a] Sulfate was below the detection limit.
[b] The uncertainties are the standard deviations of γ from duplicate experiments.

of the reasons behind it, we can conclude that the precipitation of less soluble $CaSO_4$ promoted sulfate formation.

3.4 Reactive uptake coefficient of SO_2

The reactive uptake coefficients of SO_2 (γ) for sulfate formation under different conditions are shown in Table 2. Each reaction was repeated three times, during which three particles with different sizes were selected. γ was higher at higher relative humidity, suggesting again that water in the aqueous solution plays an important role in the formation of $CaSO_4$. At 17 % RH, the reaction between $CaCO_3$ and NO_2 (the first process of the whole reaction) proceeded very slowly, and the amount of water in the aqueous solution formed due to the water uptake of $Ca(NO_3)_2$ was very low. As a result, we did not observe the formation of $CaSO_4$ (the second process of the whole reaction) after 1000 min of the reaction and even at higher SO_2 and NO_2 concentrations (200 ppm SO_2, 200 ppm NO_2). Under higher relative humidity (46 and 72 % RH), sulfate was observed soon after the reaction. It is interesting to note that there were no significant differences for γ between 46 and 72 % RH. In either case, the reaction between $CaCO_3$ and NO_2 proceeded quickly, and $CaCO_3$ was completely converted to a $Ca(NO_3)_2$ droplet within 100 min of the reaction. In the presence of enough water in the aqueous solution, RH no longer seemed to be a limiting factor. In such conditions, an increase of NO_2 concentration (from 75 to 200 ppm at 72 % RH) promoted the reactive uptake of SO_2.

The reactive uptake coefficient of SO_2 for sulfate formation was determined to be on the order of 10^{-8} at 46 and 72 % RH. This value is higher than the uptake coefficient (10^{-10}) on mineral particles sampled from the islands of Cabo Verde (the main contents being potassium feldspars and quartz) obtained by Ullerstam et al. (2003) using NO_2 / SO_2 mixing gas and the diffuse reflectance infrared Fourier transform spectroscopy (DRIFTS) technique. But the uptake coefficient in this study is lower than the uptake coefficient of SO_2 on Arizona test dust (ATD) particles in the presence of NO_2 ($(2.10 \pm 0.08) \times 10^{-6}$) determined by Park and Jang (2016). γ here is also much lower than the γ of SO_2 on oxalic acid particles in the presence of NO_2 and NH_3 (10^{-6}–10^{-4}) determined at varying RH reported by Wang et al. (2016). The difference in these uptake coefficients is attributed to the different chemical composition of particles, reaction mechanism, reaction conditions, and the ways that the particle surface is determined. It is worth noting that in the studies of Ullerstam et al. (2003) and Park and Jang (2016), particles exist in the solid state, and sulfate formation is via gas–solid heterogeneous reaction, and in the study of Wang et al. (2016) sulfate formation is stated to be via aqueous reaction. In this study sulfate formation was via gas–liquid–solid multiphase reaction, and water in the aqueous solution played a key role.

The γ of SO_2 was further compared with the reaction rate constants of the aqueous reaction of NO_2 with sulfite and bisulfite in bulk solution in the literature by deriving γ from rate constants using the method in Davidovits et al. (2006). Details of this method can be referred to in Sect. S1. Lee and Schwartz (1983) determined the rate constant of the reaction of NO_2 with bisulfite to be $> 2 \times 10^6$ mol^{-1} L s^{-1} at pH 5.8 and 6.4. Clifton et al. (1988) determined the rate constant of the reaction of NO_2 with sulfite/bisulfite to be (1.24–2.95) $\times 10^7$ mol^{-1} L s^{-1} at pH 5.6–13 and further reported a rate constant of 1.4×10^5 mol^{-1} L s^{-1} at pH 5 from the study of Lee and Schwartz (1983). The different rate constants were attributed to the different approaches of determining the reaction rate by Clifton et al. (1988). Clifton et al. (1988) determined the reaction rate from the consumption rate of the reactant, NO_2, which corresponds to the first reaction step of NO_2 with S(IV). However, Lee and Schwartz (1983) determined the reaction rate from the production rate of products (their conductivity), which is expected to be much slower than NO_2 consumption since the formation of products needs more steps. In this study, we determined γ using the sulfate production rate, and thus our data are comparable to the study of Lee and Schwartz (1983). However, the study of Lee and Schwartz (1983) only covers a pH range of 5–6.4 and has no overlap with the pH (~ 3) in our study, therefore uptake coefficients from both studies are not directly comparable. Nevertheless, the reaction rate of 1.4×10^5 mol^{-1} L s^{-1} at pH 5 corresponds to the uptake coefficient of 4.3×10^{-7}, which is around 1 order of magnitude higher than the uptake coefficient in our study determined at pH ~ 3 for the droplet. The difference may be due to the different pH between these two studies, the different mechanisms between the multiphase reaction on particles and the bulk aqueous reaction, and the different concentrations of each S(IV) species since the different species may have a different reactivity with NO_2. The reaction rate of S(IV) has been found to decrease with decreasing pH, and the reactivity of sulfite with NO_2 seems to be higher than bisulfite (Lee and Schwartz, 1983; Clifton et al., 1988; Takeuchi et al., 1977). In addition, the ionic strength in the droplet of this study (15–55 mol kg^{-1}) was much higher than that in the bulk solution in previous studies (on the order of 10^{-6}–10^{-1} mol kg^{-1}), which may also influence the reaction rate.

In the ambient atmosphere, the reactive uptake coefficient of SO_2 due to the multiphase oxidation by NO_2 is influenced by various factors such as RH, NO_2 concentration, pH, sulfate concentration, and the presence of other ions in aerosol particles. For example, NO_2 concentrations in the atmosphere are much lower than those used in this study. At lower NO_2 concentrations, the uptake coefficient of SO_2 decreases, because the oxidation rate of SO_2 in the aqueous phase decreases with decreasing NO_2 concentration. In addition, aqueous sulfate concentrations in aerosol particles in the atmosphere are often high. According to the effect of cations (Sect. 3.3.2), while reduced sulfate concentration by $CaSO_4$ precipitation likely led to the enhanced sulfate production rate in the reaction of SO_2 on $Ca(NO_3)_2$, higher sulfate concentration could increase the reaction Gibbs energy $\Delta_r G$ (as shown in Eq. 5) and reduce the colliding probability of S(IV) species with NO_2 in the aqueous phase as discussed above and thus suppress the reaction of SO_2 and NO_2. This can reduce the uptake coefficient of SO_2. Therefore, the reactive uptake coefficient of SO_2 obtained in this study (10^{-8} at 46–72 % RH and 75 ppm NO_2) can be regarded as an upper limit of the reactive uptake coefficient of SO_2 due to the multiphase reaction with NO_2 in the ambient atmosphere.

4 Conclusion and implications

We investigated the heterogeneous reaction of SO_2 directly with NO_2 on individual $CaCO_3$ particles in N_2 using Micro-Raman spectrometry. The reaction first converted the $CaCO_3$ particle to the $Ca(NO_3)_2$ droplet via the reaction with NO_2 in the SO_2 / NO_2 / H_2O / N_2 gas mixture and the deliquescence of $Ca(NO_3)_2$, and then it formed needle-shaped $CaSO_4$ crystals in the $Ca(NO_3)_2$ droplet via the multiphase reaction of SO_2 with NO_2. The sulfate formation was observed only during the multiphase oxidation by NO_2, that is, after the complete conversion of $CaCO_3$ to $Ca(NO_3)_2$ droplet. The precipitation of $CaSO_4$ from a solution promoted sulfate formation. The reactive uptake coefficient of SO_2 for sulfate formation in the multiphase reaction with NO_2 is on the order of 10^{-8} under the experimental conditions of this study (RH: 46–72 %, NO_2: 75 ppm). The reactive uptake coefficient of SO_2 was found to be enhanced at higher RH.

In order to assess the importance of the multiphase reaction of SO_2 directly oxidized by NO_2 to sulfate in the atmosphere, we compare the lifetime of SO_2 due to the multiphase oxidation of SO_2 by NO_2 with the lifetime due to the gas-phase oxidation of SO_2 by OH. Using a daytime OH concentration of 1×10^6 molecule cm^{-3} (Lelieveld et al., 2016; Prinn et al., 2005), the lifetime of SO_2 in the atmosphere due to gas-phase OH oxidation is around 12 days. The lifetime of SO_2 due to the multiphase oxidation by NO_2 is around 7000 days using the uptake coefficient of SO_2 from this study (3.22×10^{-8}) and a typical particle surface area concentration for mineral aerosols in winter in Beijing (6.3×10^{-6} cm^2 cm^{-3}) (Huang et al., 2015). Using an annual average particle surface area concentration of PM_{10} in Beijing (1.4×10^{-5} cm^2 cm^{-3}) (Wehner et al., 2008) results in a SO_2 lifetime of 3300 days due to the multiphase oxidation by NO_2. In the atmosphere, the lifetime of SO_2 due to the multiphase oxidation by NO_2 should be even longer than these values because the uptake coefficient of SO_2 used here (3.22×10^{-8}) is an upper limit of the uptake coefficient of SO_2 in the ambient atmosphere as discussed above. This comparison indicates that the direct multiphase oxidation of SO_2 by NO_2 is unlikely to be an important sink of SO_2 and source of sulfate compared with the oxidation of SO_2 by OH.

It is worth mentioning that this study did not investigate the dependence of the reactive uptake coefficient due to the direct oxidation of SO_2 by NO_2 on pH, especially not under high pH conditions, for which recent studies have claimed this reaction to be important (Cheng et al., 2016; Wang et al., 2016). Because of the important role of multiphase/heterogeneous reactions in SO_2 oxidation found in the atmosphere and the low reaction rate of the direct multiphase oxidation of SO_2 by NO_2, it is more likely that the aqueous reactions of SO_2 with other oxidants, such as the reactions with H_2O_2, O_3, and O_2, with or without transition metals, could be important pathways for sulfate formation in the atmosphere.

Data availability. The data in the figures in both the main text and the supplement are available upon request to the corresponding author (tzhu@pku.edu.cn).

The Supplement related to this article is available online at https://doi.org/10.5194/acp-18-2481-2018-supplement.

Competing interests. The authors declare that they have no conflict of interest.

Acknowledgements. This work was supported by the Natural Science Foundation Committee of China (41421064, 21190051, and 40490265) and the Ministry of Science and Technology (grant no. 2002CB410802).

Edited by: Markus Ammann
Reviewed by: three anonymous referees

References

Al-Abadleh, H. A., Krueger, B. J., Ross, J. L., and Grassian, V. H.: Phase transitions in calcium nitrate thin films, Chem. Commun., 2003, 2796–2797, https://doi.org/10.1039/B308632A, 2003.

Cao, J. J., Lee, S. C., Zhang, X. Y., Chow, J. C., An, Z. S., Ho, K. F., Watson, J. G., Fung, K., Wang, Y. Q., and Shen, Z. X.: Characterization of airborne carbonate over a site near Asian dust source regions during spring 2002 and its climatic and environmental significance, J. Geophys. Res., 110, D03203, https://doi.org/10.1029/2004jd005244, 2005.

Cheng, Y. F., Zheng, G. J., Wei, C., Mu, Q., Zheng, B., Wang, Z. B., Gao, M., Zhang, Q., He, K. B., Carmichael, G., Pöschl, U., and Su, H.: Reactive nitrogen chemistry in aerosol water as a source of sulfate during haze events in China, Science Advances, 2, e1601530, https://doi.org/10.1126/sciadv.1601530, 2016.

Chu, B., Zhang, X., Liu, Y., He, H., Sun, Y., Jiang, J., Li, J., and Hao, J.: Synergetic formation of secondary inorganic and organic aerosol: effect of SO_2 and NH_3 on particle formation and growth, Atmos. Chem. Phys., 16, 14219–14230, https://doi.org/10.5194/acp-16-14219-2016, 2016.

Clifton, C. L., Altstein, N., and Huie, R. E.: Rate-constant for the reaction of NO_2 with sulfur(IV) over the pH range 5.3–13, Environ. Sci. Technol., 22, 586–589, https://doi.org/10.1021/es00170a018, 1988.

Cui, H. X., Cheng, T. T., Chen, J. M., Xu, Y. F., and Fang, W.: A Simulated Heterogeneous Reaction of SO_2 on the Surface of Hematite at Different Temperatures, Acta Physico-Chimica Sinica, 24, 2331–2336, https://doi.org/10.3866/pku.whxb20081231, 2008.

Davidovits, P., Kolb, C. E., Williams, L. R., Jayne, J. T., and Worsnop, D. R.: Mass accommodation and chemical reactions at gas-liquid interfaces, Chem. Rev., 106, 1323–1354, https://doi.org/10.1021/cr040366k, 2006.

Ellison, T. K. and Eckert, C. A.: The oxidation of aqueous sulfur dioxide. 4. The influence of nitrogen dioxide at low pH, J. Phys. Chem., 88, 2335–2339, https://doi.org/10.1021/j150655a030, 1984.

Finlayson-Pitts, B. and Pitts Jr., J.: Chemistry of the upper and lower atmosphere: theory, experiments, and applications, Academic Press, San Diego, 969 pp., 1999.

Fu, X., Wang, S. X., Chang, X., Cai, S. Y., Xing, J., and Hao, J. M.: Modeling analysis of secondary inorganic aerosols over China: pollution characteristics, and meteorological and dust impacts, Scientific Reports, 6, 35992, https://doi.org/10.1038/srep35992, 2016.

Gao, M., Carmichael, G. R., Wang, Y., Ji, D., Liu, Z., and Wang, Z.: Improving simulations of sulfate aerosols during winter haze over Northern China: the impacts of heterogeneous oxidation by NO_2, Front. Env. Sci. Eng., 10, 16, https://doi.org/10.1007/s11783-016-0878-2, 2016.

Good, R. J. and Koo, M. N.: Effect of drop size on contact-angle, J. Colloid Interf. Sci., 71, 283–292, 1979.

Goodman, A. L., Li, P., Usher, C. R., and Grassian, V. H.: Heterogeneous uptake of sulfur dioxide on aluminum and magnesium oxide particles, J. Phys. Chem. A, 105, 6109–6120, 2001.

Guo, S., Hu, M., Zamora, M. L., Peng, J., Shang, D., Zheng, J., Du, Z., Wu, Z., Shao, M., Zeng, L., Molina, M. J., and Zhang, R.: Elucidating severe urban haze formation in China, P. Natl. Acad. Sci. USA, 111, 17373–17378, https://doi.org/10.1073/pnas.1419604111, 2014.

He, H., Wang, Y., Ma, Q., Ma, J., Chu, B., Ji, D., Tang, G., Liu, C., Zhang, H., and Hao, J.: Mineral dust and NO_x promote the conversion of SO_2 to sulfate in heavy pollution days, Scientific Reports, 4, 4172, https://doi.org/10.1038/srep04172, 2014.

Huang, L., Zhao, Y., Li, H., and Chen, Z.: Kinetics of Heterogeneous Reaction of Sulfur Dioxide on Authentic Mineral Dust: Effects of Relative Humidity and Hydrogen Peroxide, Environ. Sci. Technol., 49, 10797–10805, https://doi.org/10.1021/acs.est.5b03930, 2015.

Huang, L. B., Zhao, Y., Li, H., and Chen, Z. M.: Hydrogen peroxide maintains the heterogeneous reaction of sulfur dioxide on mineral dust proxy particles, Atmos. Environ., 141, 552–559, https://doi.org/10.1016/j.atmosenv.2016.07.035, 2016.

Huang, X., Song, Y., Zhao, C., Li, M., Zhu, T., Zhang, Q., and Zhang, X.: Pathways of sulfate enhancement by natural and anthropogenic mineral aerosols in China, J. Geophys. Res.-Atmos., 119, 14165–114179, https://doi.org/10.1002/2014jd022301, 2014.

Hwang, H. J. and Ro, C. U.: Direct observation of nitrate and sulfate formations from mineral dust and sea-salts using low-Z particle electron probe X-ray microanalysis, Atmos. Environ., 40, 3869–3880, https://doi.org/10.1016/j.atmosenv.2006.02.022, 2006.

Kong, L. D., Zhao, X., Sun, Z. Y., Yang, Y. W., Fu, H. B., Zhang, S. C., Cheng, T. T., Yang, X., Wang, L., and Chen, J. M.: The effects of nitrate on the heterogeneous uptake of sulfur dioxide on hematite, Atmos. Chem. Phys., 14, 9451–9467, https://doi.org/10.5194/acp-14-9451-2014, 2014.

Krueger, B. J., Grassian, V. H., Cowin, J. P., and Laskin, A.: Heterogeneous chemistry of individual mineral dust particles from different dust source regions: the importance of particle mineralogy, Atmos. Environ., 38, 6253–6261, https://doi.org/10.1016/j.atmosenv.2004.07.010, 2004.

Laskin, A., Iedema, M. J., Ichkovich, A., Graber, E. R., Taraniuk, I., and Rudich, Y.: Direct observation of completely processed calcium carbonate dust particles, Faraday Discuss., 130, 453-468, https://doi.org/10.1039/b417366j, 2005.

Lee, Y.-N. and Schwartz, S. E.: Kinetics of oxidation of aqueous sulfur (IV) by nitrogen dioxide, in: Precipitation Scavenging, Dry Deposition and Resuspension, edited by: Pruppacher, H. R., Semonin, R. G., and Slinn, W. G. N., Elsevier, New York, 453–466, 1983.

Lelieveld, J., Gromov, S., Pozzer, A., and Taraborrelli, D.: Global tropospheric hydroxyl distribution, budget and reactivity, Atmos. Chem. Phys., 16, 12477–12493, https://doi.org/10.5194/acp-16-12477-2016, 2016.

Li, H. J., Zhu, T., Zhao, D. F., Zhang, Z. F., and Chen, Z. M.: Kinetics and mechanisms of heterogeneous reaction of NO_2 on $CaCO_3$ surfaces under dry and wet conditions, Atmos. Chem. Phys., 10, 463–474, https://doi.org/10.5194/acp-10-463-2010, 2010.

Li, J., Shang, J., and Zhu, T.: Heterogeneous reactions of SO_2 on ZnO particle surfaces, Sci. China Chem., 54, 161–166, https://doi.org/10.1007/s11426-010-4167-9, 2011.

Li, L., Chen, Z. M., Ding, J., Zhu, T., and Zhang, Y. H.: A DRIFTS study of SO_2 oxidation on the surface of $CaCO_3$ particles, Spectrosc. Spect. Anal., 24, 1556–1559, 2004.

Li, L., Chen, Z. M., Zhang, Y. H., Zhu, T., Li, J. L., and Ding, J.: Kinetics and mechanism of heterogeneous oxidation of sulfur dioxide by ozone on surface of calcium carbonate, Atmos. Chem. Phys., 6, 2453–2464, https://doi.org/10.5194/acp-6-2453-2006, 2006.

Li, L., Chen, Z. M., Zhang, Y. H., Zhu, T., Li, S., Li, H. J., Zhu, L. H., and Xu, B. Y.: Heterogeneous oxidation of sulfur dioxide by ozone on the surface of sodium chloride and its mixtures with other components, J. Geophys. Res., 112, D18301, https://doi.org/10.1029/2006jd008207, 2007.

Li, W. J. and Shao, L. Y.: Observation of nitrate coatings on atmospheric mineral dust particles, Atmos. Chem. Phys., 9, 1863–1871, https://doi.org/10.5194/acp-9-1863-2009, 2009.

Lide, D. R.: CRC Handbook of Chemistry and Physics, 89th Edn., CRC Press/Taylor and Francis, Boca Raton, FL, 2009.

Littlejohn, D., Wang, Y. Z., and Chang, S. G.: Oxidation of aqueous sulfite ion by nitrogen-dioxide, Environ. Sci. Technol., 27, 2162–2167, https://doi.org/10.1021/es00047a024, 1993.

Liu, C., Ma, Q. X., Liu, Y. C., Ma, J. Z., and He, H.: Synergistic reaction between SO_2 and NO_2 on mineral oxides: a potential formation pathway of sulfate aerosol, Phys. Chem. Chem. Phys., 14, 1668–1676, https://doi.org/10.1039/c1cp22217a, 2012.

Liu, Y. J., Zhu, T., Zhao, D. F., and Zhang, Z. F.: Investigation of the hygroscopic properties of $Ca(NO_3)_2$ and internally mixed $Ca(NO_3)_2/CaCO_3$ particles by micro-Raman spectrometry, Atmos. Chem. Phys., 8, 7205–7215, https://doi.org/10.5194/acp-8-7205-2008, 2008.

Ma, Q., He, H., Liu, Y., Liu, C., and Grassian, V. H.: Heterogeneous and multiphase formation pathways of gypsum in the atmosphere, Phys. Chem. Chem. Phys., 15, 19196–19204, https://doi.org/10.1039/c3cp53424c, 2013.

Ma, Q., Wang, T., Liu, C., He, H., Wang, Z., Wang, W., and Liang, Y.: SO_2 Initiates the Efficient Conversion of NO_2 to HONO on MgO Surface, Environ. Sci. Technol., 51, 3767–3775, https://doi.org/10.1021/acs.est.6b05724, 2017.

Ma, Q. X., Liu, Y. C., and He, H.: Synergistic effect between NO_2 and SO_2 in their adsorption and reaction on gamma-alumina, J. Phys. Chem. A, 112, 6630–6635, https://doi.org/10.1021/jp802025z, 2008.

Ma, Q. X., He, H., Liu, Y. C., Liu, C., and Grassian, V. H.: Heterogeneous and multiphase formation pathways of gypsum in the atmosphere, Phys. Chem. Chem. Phys., 15, 19196–19204, https://doi.org/10.1039/c3cp53424c, 2013.

Martin, L. R., Damschen, D. E., and Judeikis, H. S.: The reactions of nitrogen-oxides with SO_2 in aqueous aerosols, Atmos. Environ., 15, 191–195, https://doi.org/10.1016/0004-6981(81)90010-x, 1981.

Meyer, B., Ospina, M., and Peter, L. B.: Raman spectrometric determination of oxysulfur anions in aqueous systems, Anal. Chim. Acta, 117, 301–311, https://doi.org/10.1016/0003-2670(80)87030-9, 1980.

Nakamoto, K.: Infrared and Raman Spectra of Inorganic and Coordination Compounds, John Wiley & Sons, New York, 1997.

Nash, T.: Effect of nitrogen-dioxide and of some transition-metals on the oxidation of dilute bisulfite solutions, Atmos. Environ., 13, 1149–1154, https://doi.org/10.1016/0004-6981(79)90038-6, 1979.

Okada, K., Qin, Y., and Kai, K.: Elemental composition and mixing properties of atmospheric mineral particles collected in Hohhot, China, Atmos. Res., 73, 45–67, 2005.

Park, J. Y. and Jang, M.: Heterogeneous photooxidation of sulfur dioxide in the presence of airborne mineral dust particles, RSC Adv., 6, 58617–58627, https://doi.org/10.1039/c6ra09601h, 2016.

Passananti, M., Kong, L. D., Shang, J., Dupart, Y., Perrier, S., Chen, J. M., Donaldson, D. J., and George, C.: Organosulfate Formation through the Heterogeneous Reaction of Sulfur Dioxide with Unsaturated Fatty Acids and Long-Chain Alkenes, Angew. Chem. Int. Edit., 55, 10336–10339, https://doi.org/10.1002/anie.201605266, 2016.

Prince, A. P., Grassian, V. H., Kleiber, P., and Young, M. A.: Heterogeneous conversion of calcite aerosol by nitric acid, Phys. Chem. Chem. Phys., 9, 622–634, 2007a.

Prince, A. P., Kleiber, P., Grassian, V. H., and Young, M. A.: Heterogeneous interactions of calcite aerosol with sulfur dioxide and sulfur dioxide-nitric acid mixtures, Phys. Chem. Chem. Phys., 9, 3432–3439, 2007b.

Prinn, R. G., Huang, J., Weiss, R. F., Cunnold, D. M., Fraser, P. J., Simmonds, P. G., McCulloch, A., Harth, C., Reimann, S., Salameh, P., O'Doherty, S., Wang, R. H. J., Porter, L. W., Miller, B. R., and Krummel, P. B.: Evidence for variability of atmospheric hydroxyl radicals over the past quarter century, Geophys. Res. Lett., 32, L07809, https://doi.org/10.1029/2004gl022228, 2005.

Rosenberg, H. S. and Grotta, H. M.: Nitrogen oxides (NO_x) influence on sulfite oxidation and scaling in lime/limestone flue gas desulfurization (FGD) systems, Environ. Sci. Technol., 14, 470–472, https://doi.org/10.1021/es60164a011, 1980.

Sarma, L. P., Prasad, P. S. R., and Ravikumar, N.: Raman spectroscopic study of phase transitions in natural gypsum, J. Raman Spectrosc., 29, 851–856, https://doi.org/10.1002/(sici)1097-4555(199809)29:9<851::aid-jrs313>3.0.co;2-s, 1998.

Seinfeld, J. H. and Pandis, S. N.: Atmospheric chemistry and physics: from air pollution to climate change, 2nd Edn., John Wiley & Sons. Inc., 2006.

Shang, J., Li, J., and Zhu, T.: Heterogeneous reaction of SO_2 on TiO_2 particles, Sci. China Chem., 53, 2637–2643, https://doi.org/10.1007/s11426-010-4160-3, 2010.

Shen, C. H. and Rochelle, G. T.: Nitrogen Dioxide Absorption and Sulfite Oxidation in Aqueous Sulfite, Environ. Sci. Technol., 32, 1994–2003, https://doi.org/10.1021/es970466q, 1998.

Song, C. H., Maxwell-Meier, K., Weber, R. J., Kapustin, V., and Clarke, A.: Dust composition and mixing state inferred from airborne composition measurements during ACE-Asia C130 Flight #6, Atmos. Environ., 39, 359–369, 2005.

Sorimachi, A., Sakai, M., Ishitani, O., Nishikawa, M., and Sakamoto, K.: Study on dry deposition of SO_2-NO_x onto loess, Water Air Soil Pollut., 130, 541–546, https://doi.org/10.1023/a:1013834729728, 2001.

Stafford, R. G., Chang, R. K., and Kindlmann, P. J.: Laser-Raman monitoring of ambient sulfate aerosols, in: Methods and standards for environmentalmeasurement: Proceedings of the 8th Materials Research Symposium, Gaithersburg, Maryland, USA, 20–24 September 1976, edited by: Kirchhoff, W. H., National Bureau of Standards, Washington, 1976.

Sullivan, R. C., Guazzotti, S. A., Sodeman, D. A., and Prather, K. A.: Direct observations of the atmospheric processing of Asian mineral dust, Atmos. Chem. Phys., 7, 1213–1236, https://doi.org/10.5194/acp-7-1213-2007, 2007.

Takeuchi, H., Ando, M., and Kizawa, N.: Absorption of Nitrogen Oxides in Aqueous Sodium Sulfite and Bisulfite Solutions, In. Eng. Chem. Proc. D.D., 16, 303–308, https://doi.org/10.1021/i260063a010, 1977.

Tan, F., Jing, B., Tong, S. R., and Ge, M. F.: The effects of coexisting Na_2SO_4 on heterogeneous uptake of NO_2 on $CaCO_3$ particles at various RHs, Sci. Total Environ., 586, 930–938, https://doi.org/10.1016/j.scitotenv.2017.02.072, 2017.

Tang, I. N. and Fung, K. H.: Hydration and Raman scattering studies of levitated microparticles: $Ba(NO_3)_2$, $Sr(NO_3)_2$, and $Ca(NO_3)2$, J. Chem. Phys., 106, 1653–1660, 1997.

Tursic, J. and Grgic, I.: Influence of NO_2 on S(IV) oxidation in aqueous suspensions of aerosol particles from two different origins, Atmos. Environ., 35, 3897–3904, https://doi.org/10.1016/s1352-2310(01)00142-x, 2001.

Ullerstam, M., Vogt, R., Langer, S., and Ljungstrom, E.: The kinetics and mechanism of SO_2 oxidation by O_3 on mineral dust, Phys. Chem. Chem. Phys., 4, 4694–4699, https://doi.org/10.1039/b203529b, 2002.

Ullerstam, M., Johnson, M. S., Vogt, R., and Ljungström, E.: DRIFTS and Knudsen cell study of the heterogeneous reactivity of SO_2 and NO_2 on mineral dust, Atmos. Chem. Phys., 3, 2043–2051, https://doi.org/10.5194/acp-3-2043-2003, 2003.

Wang, G., Zhang, R., Gomez, M. E., Yang, L., Levy Zamora, M., Hu, M., Lin, Y., Peng, J., Guo, S., Meng, J., Li, J., Cheng, C., Hu, T., Ren, Y., Wang, Y., Gao, J., Cao, J., An, Z., Zhou, W., Li, G., Wang, J., Tian, P., Marrero-Ortiz, W., Secrest, J., Du, Z., Zheng, J., Shang, D., Zeng, L., Shao, M., Wang, W., Huang, Y., Wang, Y., Zhu, Y., Li, Y., Hu, J., Pan, B., Cai, L., Cheng, Y., Ji, Y., Zhang, F., Rosenfeld, D., Liss, P. S., Duce, R. A., Kolb, C. E., and Molina, M. J.: Persistent sulfate formation from London Fog to Chinese haze, P. Natl. Acad. Sci. USA, 113, 13630–13635, https://doi.org/10.1073/pnas.1616540113, 2016.

Wang, Y. S., Yao, L., Wang, L. L., Liu, Z. R., Ji, D. S., Tang, G. Q., Zhang, J. K., Sun, Y., Hu, B., and Xin, J. Y.: Mechanism for the formation of the January 2013 heavy haze pollution episode over central and eastern China, Sci. China Earth Sci., 57, 14–25, https://doi.org/10.1007/s11430-013-4773-4, 2014.

Wang, Y. X., Zhang, Q. Q., Jiang, J. K., Zhou, W., Wang, B. Y., He, K. B., Duan, F. K., Zhang, Q., Philip, S., and Xie, Y. Y.: Enhanced sulfate formation during China's severe winter haze episode in January 2013 missing from current models, J. Geophys. Res.-Atmos., 119, 10425–10440, https://doi.org/10.1002/2013jd021426, 2014.

Wehner, B., Birmili, W., Ditas, F., Wu, Z., Hu, M., Liu, X., Mao, J., Sugimoto, N., and Wiedensohler, A.: Relationships between submicrometer particulate air pollution and air mass history in Beijing, China, 2004–2006, Atmos. Chem. Phys., 8, 6155–6168, https://doi.org/10.5194/acp-8-6155-2008, 2008.

Wright, M. L.: Feasibility study of in-situ souce monitoring of particulate composition by Raman or fluorescence scatter, U.S. Environmental Protection Agency, Washington, D.C., 1973.

Wu, L. Y., Tong, S. R., Wang, W. G., and Ge, M. F.: Effects of temperature on the heterogeneous oxidation of sulfur dioxide by ozone on calcium carbonate, Atmos. Chem. Phys., 11, 6593–6605, https://doi.org/10.5194/acp-11-6593-2011, 2011.

Wu, L. Y., Tong, S. R., Zhou, L., Wang, W. G., and Ge, M. F.: Synergistic Effects between SO_2 and HCOOH on α-Fe_2O_3, J. Phys. Chem. A, 117, 3972–3979, https://doi.org/10.1021/jp400195f, 2013.

Wu, L. Y., Tong, S. R., and Ge, M. F.: Synergistic Effect between SO_2 and HCOOH on the Surface of CaO, Acta Chim. Sinica 73, 131–136, https://doi.org/10.6023/a14120875, 2015.

Xie, Y. N., Ding, A. J., Nie, W., Mao, H. T., Qi, X. M., Huang, X., Xu, Z., Kerminen, V. M., Petaja, T., Chi, X. G., Virkkula, A., Boy, M., Xue, L. K., Guo, J., Sun, J. N., Yang, X. Q., Kulmala, M., and Fu, C. B.: Enhanced sulfate formation by nitrogen dioxide: Implications from in situ observations at the SORPES station, J. Geophys. Res.-Atmos., 120, 12679–12694, https://doi.org/10.1002/2015jd023607, 2015.

Xue, J., Yuan, Z. B., Griffith, S. M., Yu, X., Lau, A. K. H., and Yu, J. Z.: Sulfate Formation Enhanced by a Cocktail of High NO_x, SO_2, Particulate Matter, and Droplet pH during Haze-Fog Events in Megacities in China: An Observation-Based Modeling Investigation, Environ. Sci. Technol., 50, 7325–7334, https://doi.org/10.1021/acs.est.6b00768, 2016.

Zhang, D. Z., Shi, G. Y., Iwasaka, Y., and Hu, M.: Mixture of sulfate and nitrate in coastal atmospheric aerosols: individual particle studies in Qingdao (36°04′ N, 120°21′ E), China, Atmos. Environ., 34, 2669–2679, https://doi.org/10.1016/s1352-2310(00)00078-9, 2000.

Zhang, D. Z., Zang, J. Y., Shi, G. Y., Iwasaka, Y., Matsuki, A., and Trochkine, D.: Mixture state of individual Asian dust particles at a coastal site of Qingdao, China, Atmos. Environ., 37, 3895–3901, https://doi.org/10.1016/s1352-2310(03)00506-5, 2003.

Zhang, J. K., Sun, Y., Liu, Z. R., Ji, D. S., Hu, B., Liu, Q., and Wang, Y. S.: Characterization of submicron aerosols during a month of serious pollution in Beijing, 2013, Atmos. Chem. Phys., 14, 2887–2903, https://doi.org/10.5194/acp-14-2887-2014, 2014.

Zhang, Q., Jimenez, J. L., Canagaratna, M. R., Allan, J. D., Coe, H., Ulbrich, I., Alfarra, M. R., Takami, A., Middlebrook, A. M., Sun, Y. L., Dzepina, K., Dunlea, E., Docherty, K., DeCarlo, P. F., Salcedo, D., Onasch, T., Jayne, J. T., Miyoshi, T., Shimono, A., Hatakeyama, S., Takegawa, N., Kondo, Y., Schneider, J., Drewnick, F., Borrmann, S., Weimer, S., Demerjian, K., Williams, P., Bower, K., Bahreini, R., Cottrell, L., Griffin, R. J., Rautiainen, J., Sun, J. Y., Zhang, Y. M., and Worsnop, D. R.: Ubiquity and dominance of oxygenated species in organic aerosols in anthropogenically-influenced Northern Hemisphere midlatitudes, Geophys. Res. Lett., 34, L13801, https://doi.org/10.1029/2007gl029979, 2007.

Zhao, D. F., Zhu, T., Chen, Q., Liu, Y. J., and Zhang, Z. F.: Raman micro-spectrometry as a technique for investigating heterogeneous reactions on individual atmospheric particles, Sci. China Chem., 54, 154–160, https://doi.org/10.1007/s11426-010-4182-x, 2011.

Zhao, X., Kong, L. D., Sun, Z. Y., Ding, X. X., Cheng, T. T., Yang, X., and Chen, J. M.: Interactions between Heterogeneous Uptake and Adsorption of Sulfur Dioxide and Acetaldehyde on Hematite, J. Phys. Chem. A, 119, 4001-4008, https://doi.org/10.1021/acs.jpca.5b01359, 2015.

Zheng, B., Zhang, Q., Zhang, Y., He, K. B., Wang, K., Zheng, G. J., Duan, F. K., Ma, Y. L., and Kimoto, T.: Heterogeneous chemistry: a mechanism missing in current models to explain secondary inorganic aerosol formation during the January 2013 haze episode in North China, Atmos. Chem. Phys., 15, 2031–2049, https://doi.org/10.5194/acp-15-2031-2015, 2015.

Zheng, G. J., Duan, F. K., Su, H., Ma, Y. L., Cheng, Y., Zheng, B., Zhang, Q., Huang, T., Kimoto, T., Chang, D., Pöschl, U., Cheng, Y. F., and He, K. B.: Exploring the severe winter haze in Beijing: the impact of synoptic weather, regional transport and heterogeneous reactions, Atmos. Chem. Phys., 15, 2969–2983, https://doi.org/10.5194/acp-15-2969-2015, 2015.

Zhou, L., Wang, W. G., Gai, Y. B., and Ge, M. F.: Knudsen cell and smog chamber study of the heterogeneous uptake of sulfur dioxide on Chinese mineral dust, J. Environ. Sci., 26, 2423–2433, https://doi.org/10.1016/j.jes.2014.04.005, 2014.

Zhu, T., Shang, J., and Zhao, D. F.: The roles of heterogeneous chemical processes in the formation of an air pollution complex and gray haze, Sci. China Chem., 54, 145–153, https://doi.org/10.1007/s11426-010-4181-y, 2011.